Mechanism and Machine Theory 80 (2014) 125–141

Contents lists available at ScienceDirect

Mechanism and Machine Theory

journal homepage: www.elsevier.com/locate/mechmt

Optimum structural design of a two-limb Schönflies motion generator

Afshin Taghvaeipour [a,*], Jorge Angeles [a,1], Larry Lessard [b,2]

[a] Department of Mechanical Engineering and Centre for Intelligent Machines, McGill University, 817 Sherbrooke St. W., Montreal, QC H3A 2K6, Canada
[b] Department of Mechanical Engineering, McGill University, 817 Sherbrooke St. W., Montreal, QC, H3A 2K6 Canada

ARTICLE INFO

Article history:
Received 10 December 2013
Received in revised form 26 May 2014
Accepted 27 May 2014
Available online 19 June 2014

Keywords:
Schönflies motion generator
Stiffness
Optimization
Sensitivity analysis

ABSTRACT

The optimum dimensions of a two-limb Schönflies motion generator, to maximize the overall stiffness of the robot structure is the subject of this paper. In the six-dimensional Cartesian space, for a mechanical system, six independent stiffnesses can be defined: three translational along three independent directions and three rotational about axes parallel to these directions. In this study, the objective is to maximize the maximum translational and rotational stiffnesses when the robot is at a specific pose. To this end, first, the stiffness matrix of the robot is obtained using the concept of the generalized spring; second, by introducing the translational and rotational stiffness indices κ_t and κ_r, respectively, two objective functions are defined. For the optimization procedure, a genetic algorithm (GA) is used. As a result, three different designs are introduced, their stiffness performance over a test trajectory then being analyzed. At the end, the sensitivity analysis of the robot stiffness with respect to some design parameters is studied.

1. Introduction

Engineers are always seeking for an optimum design; this includes either minimization of a cost or maximization of a profit with or without constraints. A real-life engineering optimization problem usually consists of a number of conflicting objective functions and constraints with many design variables, which calls for multi-objective optimization. Generally, optimization procedures are divided into two main categories, gradient and non-gradient methods. The former are based on the calculation of derivatives of the objective and constraint functions, the latter only on function evaluation. In most engineering problems, objective and constraint functions are so complex that they cannot be described by formulas, the calculation of their derivatives being impossible. Hence, *direct* methods, not requiring gradients, are commonly used for this type of problems. Many direct methods are available, e.g., *Genetic Algorithms* (GAs) [1], *Simulated Annealing* (SA) [2], and *The Complex Method* [3], among the best known. The optimization of robot manipulators has been studied for many years. Performance improvement of robotic systems is one of the important issues being addressed in recent years. Stock et al. conducted a kinematic optimization method for parallel manipulators; they applied the method on the Linear Delta robot [4]. Ceccarelli et al. investigated a multi-objective optimization problem on general 3R manipulators [5]. In the foregoing paper,

* Corresponding author. Tel.: +1 514 398 3938; fax: +1 514 398 7348.
E-mail addresses: afshin.taghvaeipour@mail.mcgill.ca (A. Taghvaeipour), angeles@cim.mcgill.ca (J. Angeles), larry.lessard@mcgill.ca (L. Lessard).
[1] Tel.: +1 514 398 6315; fax: +1 514 398 5256.
[2] Tel.: +1 514 398 6305; fax: +1 514 398 7365.

http://dx.doi.org/10.1016/j.mechmachtheory.2014.05.005
0094-114X/

authors considered the workspace volume and the robot dimensions as objective functions. The foregoing works mostly reported the kinematic optimization problem for robotic mechanical systems; however, in reality, to improve the overall performance of a robot its elastic behavior should also be taken into account. Liu et al. incorporated the conditioning and stiffness indices in order to obtain the optimum design of 3-dof spherical parallel manipulators [6]. In the foregoing paper the authors utilized the atlases of conditioning and stiffness indices in order to optimize the links length of the manipulator. In [7], Gao et al. targeted the design optimization of a spatial six degree-of-freedom parallel manipulator by taking into account the flexibility of the joints. By resorting to two indices which are related to system stiffness and dexterity, a multiobjective optimization problem on a spatial six degree-of-freedom parallel robot was established. In a recent study, Kelaiaia et al. considered multiple criteria of performance, such as workspace, stiffness, kinematic and dynamic, to address a multiobjective optimization problem on a linear Delta parallel robot [8]. In the foregoing papers [7,8], the multiobjective optimization problems were solved by resorting to the GAs.

This study aims at optimum design of the McGill Schönflies Motion Generator (SMG), depicted in Fig. 1, in order to enhance the robot stiffness. To evaluate the robot stiffness performance, two stiffness indices, translational and rotational, which were introduced by Taghvaeipour et al. [9], are used. By adjusting the structural parameters, such as the link lengths and the distance between the limbs, the maximization of the stiffness indices is desired. In the sequel, first, the multi-objective optimization and GA are briefly introduced, next, the stiffness matrix and the calculation technique of stiffness indices are addressed. Afterward, the specific optimization problem regarding the McGill SMG is defined. As a result, the possible optimum designs, which form a set of solutions, are shown. After the calculation of the McGill SMG optimum dimensions, in the next level, the geometry and the material optimization of the flexible components, two proximal and two distal $\prod$-joints, are the main issues. With the essential performance indices at hand, the stiffness sensitivity analysis can be an interesting topic as well. Since the latter provides an engineering insight, at the end, a novel stiffness sensitivity analysis over the McGill SMG is initiated.

2. A multi-objective optimization problem

A multi-objective optimization problem consists of a number of independent objective functions that are to be minimized or maximized [10]. In a general form, the problem can be defined as,

$$\begin{aligned} \min_{\mathbf{x}} \quad & f_m(\mathbf{x}), \quad m = 1\ldots M \\ & g_j(\mathbf{x}) \geq 0, \quad j = 1\ldots J \\ & h_k(\mathbf{x}) = 0, \quad k = 1\ldots K \\ & x_i^L < x_i < x_i^U, \quad i = 1\ldots N \end{aligned} \tag{1}$$

in which $\mathbf{x} = [x_1 \quad x_2 \quad \ldots \quad x_N]^T$ is the *design variable vector*; the objective functions can also be cast in a vector, $\mathbf{f}(\mathbf{x}) = [f_1(\mathbf{x}) \quad f_2(\mathbf{x}) \quad \ldots \quad f_M(\mathbf{x})]^T$, which is called the *objectives vector*. Accordingly, g_j and h_k are inequality and equality constraint functions, respectively. Moreover, x_i^L and x_i^U are design-variable lower and upper bounds, respectively. These bounds make design variable region $\mathscr{R}$ a hyperparallelogram. The objective functions are mostly conflicting, and hence, it is rarely feasible to find a unique solution

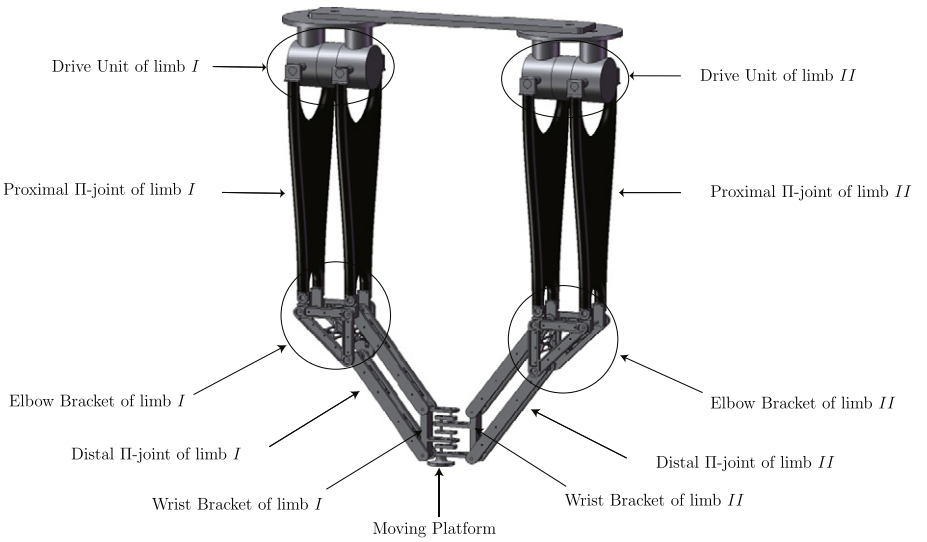

Fig. 1. The McGill SMG.

which simultaneously optimizes all objectives. Therefore, in these cases, the concept of *domination* is used [10]. According to this concept, a solution $\mathbf{x}_1$ dominates $\mathbf{x}_2$ ($\mathbf{x}_1 \succ \mathbf{x}_2$) if $\mathbf{x}_1$ is better or equal to $\mathbf{x}_2$ in all objectives, and strictly better in at least one objective. That is, for M objectives to be minimized, one has

$$\begin{aligned} &f_m(\mathbf{x}_1) \le f_m(\mathbf{x}_2), \quad \forall m = 1 \ldots M \\ &\exists m | f_m(\mathbf{x}_1) < f_m(\mathbf{x}_2), \quad m = 1 \ldots M. \end{aligned} \tag{2}$$

A set of dominant solutions and the corresponding set of objective vectors are known as the *Pareto optimal solutions* and the *Pareto optimal frontier*, respectively. In a design optimization problem, apparently, the final design should be a member of the Pareto optimal set.

3. Genetic algorithm

GAs and evolutionary algorithms were first introduced in [11,12]. In the late 80s, Goldberg developed the algorithms for solving an engineering optimization problem [1]. GA is based on the process of natural selection. Each optimization parameter is encoded into a gene, i.e., a real number or string of bits. Then, a chromosome is formed by the corresponding genes for all variables x_1, x_2, …, x_N; each chromosome describes an individual. Depending on the nature of a problem, a chromosome could be defined as an array of real numbers or a binary string. Finally, the individuals, which represent possible solutions, form a population. In the next step, the fittest individuals of a population are chosen for mating; each couple of selected individuals produces a child. The children are generated by combining genes from different parents, which is called *crossover*. At the end, a few children are chosen to mutate randomly; a procedure is called *mutation*. Finally, the new individuals form a new population and the algorithm starts all over again. The optimization procedure stops when either a maximum number of generations has been reached, or a fitness criterion has been met.

GA provides a useful tool for all kinds of optimization problems, especially for those with a number of objectives, constraint functions, and design variables that cannot be described by simple formulas. Since the early 80s, researchers developed many GA methods in multi-objective optimization problems that can be separated into two main categories: 1, non-Pareto-based approaches such as VEGA [13] and lexicographic ordering [14] and 2, Pareto-based approaches, such as SPEA [15], NSGA [16], and NSGA-II [17]. As Pareto-based approaches provide diverse solutions, they have been found to be more acceptable than their non-Pareto-based counterparts. One of the latest Pareto-based methods is NSGA-II which has been widely used since it was introduced by Deb. This method is computationally faster than others; it is based on the non-dominated sorting approach. The complete procedure can be found in [17]. Because of the foregoing merits of the NSGA-II, it is chosen as the optimization technique in this study.

4. Elastostatic analysis

Robots are made of some flexible links which are connected to each other by means of kinematic pairs. Due to different configuration of these flexible links, the robot response, "small"-amplitude displacement (SAD) screw of the moving platform (MP), to the external wrench—forces and moments—is posture-dependent. At each posture, assuming that motors are locked, the six-dimensional SAD screw of MP is mapped to the applied wrench array by means of a 6×6 matrix which is called Cartesian stiffness matrix, namely,

$$\begin{bmatrix} \mathbf{n} \\ \mathbf{f} \end{bmatrix} = \begin{bmatrix} \mathbf{K}_{11} & \mathbf{K}_{12} \\ \mathbf{K}_{12}^T & \mathbf{K}_{22} \end{bmatrix} \begin{bmatrix} \boldsymbol{\theta} \\ \boldsymbol{\sigma} \end{bmatrix} \tag{3}$$

where $\mathbf{f}$ and $\mathbf{n}$ denote force and moment, respectively, the six dimensional array of the left-hand side being a wrench; $\boldsymbol{\sigma}$ and $\boldsymbol{\theta}$ define, in turn, a "small" point-translation—small with respect to the dimensions of the system bodies—and a "small"-amplitude rotation about an axis parallel to the unit vector $\boldsymbol{\theta}/\|\boldsymbol{\theta}\|$, respectively. For robots designed for pick-and-place operations, the calculation of the Cartesian stiffness matrix is crucial, which calls for an *elastostatic analysis*. This analysis has been conducted differently, finite element analysis (FEA), the virtual joint method (VJM), and matrix structural analysis (MSA). In FEA, each component can be modeled with its actual shape. However, FEA is computationally expensive. Corradini et al. analyzed the stiffness of the H4 parallel robot by FEA, at one single posture, and the results having been experimentally verified [18]. In the second method, VJM, sometimes called *lumped-parameter method*, the compliance of the links is replaced by virtual compliant joints and rigid links [19]; then, the equivalent virtual joint stiffnesses are derived. Later, the modified version of VJM proposed in [20]; this analysis was based on a multidimensional lumped-parameter model that replaces the link compliance with localized six-dof virtual springs. The third method, MSA, is similar to FEA; instead of using a large number of elements, each part of the robot is considered as a simple structural element, beam or rod, for example [21]. Within MSA, the stiffness matrix of the structure can be obtained in parametric form, which is important when the stiffness optimization of the structure is sought. Finally, Taghvaeipour et al. proposed a method based on the well-known concept of *generalized spring* [9,22]. This method relies on a form of the enhanced MSA, with a formulation for the modeling of the six lower kinematic pairs. The concept of generalized spring appears to have first been proposed by Lončarićin the foregoing reference as a suspension for a rigid body and composed of single linearly elastic translational springs. By means of the method proposed in [9], the 6×6 Cartesian stiffness matrix of the robot can be calculated *for any robot posture*, using stiffness matrices computed offline by means of parametric, whenever possible, or numerical methods. Moreover, although the method is limited to linearly elastic structural elements, it is general enough to accommodate elastic anisotropies, as appearing in composite materials. The method is especially attractive in the realm of parallel robots with what is known as $\prod$-joints, which are *parallelogram four-bar linkages* [23,24]. As it is depicted in Fig. 1 the McGill SMG is composed of four $\prod$-joints, hence, the

generalized spring method, presented in [9] in detail, is selected in order to calculate the robot stiffness matrix. For a quick reference, this calculation is briefly explained in the Appendix A.

4.1. Stiffness indices

In order to assess the elastostatic response of a robot to an external wrench, defining stiffness indices is essential. Here, the main issue is that a 6×6 Cartesian stiffness matrix is formed by four 3×3 block matrices whose components have different units; from Eq. (3) it is apparent that the block matrices $\mathbf{K}_{11}$, $\mathbf{K}_{12}$ and $\mathbf{K}_{22}$ have units of Nm, N and N/m, respectively. To define stiffness performance indices, first we should obtain a unit-homogenized matrix from the stiffness matrix. The method used here is based on the idea introduced in [25], to define dimensionless parameters for sensitivity analysis of mechanical systems. The two three-dimensional equations Eq. (3), one for moment and one for force, are displayed below:

$$\mathbf{n} = \mathbf{K}_{11}\boldsymbol{\theta} + \mathbf{K}_{12}\boldsymbol{\sigma} \tag{4a}$$

$$\mathbf{f} = \mathbf{K}_{12}^T\boldsymbol{\theta} + \mathbf{K}_{22}\boldsymbol{\sigma}. \tag{4b}$$

Apparently, the force and moment vectors are made up of two independent components, namely,

$$\mathbf{n} = \mathbf{K}_{11}\boldsymbol{\theta} + \mathbf{K}_{12}\boldsymbol{\sigma} = \mathbf{n}_\theta + \mathbf{n}_\sigma \tag{5a}$$

$$\mathbf{f} = \mathbf{K}_{12}^T\boldsymbol{\theta} + \mathbf{K}_{22}\boldsymbol{\sigma} = \mathbf{f}_\theta + \mathbf{f}_\sigma. \tag{5b}$$

We can associate each independent part of Eq. (5b) and (5a) with a physically meaningful quadratic form [25], such as $\|\mathbf{f}_\beta\|^2 = \beta^T\mathbf{K}_\beta^T\mathbf{K}_\beta\beta$, which defines an ellipsoid in the space of β, a dummy vector variable, defined as: $\beta = \boldsymbol{\sigma}$ for a point-displacement, and $\beta = \boldsymbol{\theta}$ for a "small"-angle rotation vector. In fact, from Eq. (5a) and (5b), $\mathbf{n}$ and $\mathbf{f}$ can be defined as resistant moment and force vectors against an applied SAD; accordingly, each resistant moment and force vector is factored out into two spaces, namely, translation $\boldsymbol{\sigma}$ and rotation $\boldsymbol{\theta}$. From the above equations, it is obtained that

$$\begin{aligned} \|\mathbf{n}\|^2 &= \|\mathbf{n}_\theta\|^2 + \|\mathbf{n}_\sigma\|^2 = \boldsymbol{\theta}^T\mathbf{K}_{11}^T\mathbf{K}_{11}\boldsymbol{\theta} + \boldsymbol{\sigma}^T\mathbf{K}_{12}^T\mathbf{K}_{12}\boldsymbol{\sigma} \\ \|\mathbf{f}\|^2 &= \|\mathbf{f}_\theta\|^2 + \|\mathbf{f}_\sigma\|^2 = \boldsymbol{\theta}^T\mathbf{K}_{12}\mathbf{K}_{12}^T\boldsymbol{\theta} + \boldsymbol{\sigma}^T\mathbf{K}_{22}^T\mathbf{K}_{22}\boldsymbol{\sigma} \end{aligned} \tag{6}$$

namely,

$$\begin{aligned} \|\mathbf{n}_\theta\|^2 &= \boldsymbol{\theta}^T\mathbf{K}_{11}^T\mathbf{K}_{11}\boldsymbol{\theta}, \quad \|\mathbf{n}_\sigma\|^2 = \boldsymbol{\sigma}^T\mathbf{K}_{12}^T\mathbf{K}_{12}\boldsymbol{\sigma} \\ \|\mathbf{f}_\theta\|^2 &= \boldsymbol{\theta}^T\mathbf{K}_{12}\mathbf{K}_{12}^T\boldsymbol{\theta}, \quad \|\mathbf{f}_\sigma\|^2 = \boldsymbol{\sigma}^T\mathbf{K}_{22}^T\mathbf{K}_{22}\boldsymbol{\sigma}. \end{aligned} \tag{7}$$

Now, for each of the equations above, an eigenvalue problem can be defined, which results in three orthogonal eigenvectors $\mathbf{s}_1$, $\mathbf{s}_2$ and $\mathbf{s}_3$. These three eigenvectors span the corresponding translational or rotational spaces, namely,

$$\boldsymbol{\sigma} = \psi_1\boldsymbol{\mathcal{S}}_1 + \psi_2\boldsymbol{\mathcal{S}}_2 + \psi_3\boldsymbol{\mathcal{S}}_3 = \mathbf{S}_\sigma\psi_\sigma \tag{8}$$

where ψ_i is a dimensionless parameter and $\mathbf{S}_\sigma$ is an orthogonal transformation. Accordingly, corresponding to each eigenvalue problem presented in Eq. (7), an orthogonal transformation can be defined. Hence, we will have two linear transformations regarding the force and two for the moment equations; for the force equation the linear transformation leads to

$$\begin{bmatrix} \boldsymbol{\theta} \\ \boldsymbol{\sigma} \end{bmatrix} = \begin{bmatrix} \mathbf{S}_\theta & \mathbf{O} \\ \mathbf{O} & \mathbf{S}_\sigma \end{bmatrix} \begin{bmatrix} \psi_\theta \\ \psi_\sigma \end{bmatrix} \tag{9}$$

while, for the moment equation,

$$\begin{bmatrix} \boldsymbol{\theta} \\ \boldsymbol{\sigma} \end{bmatrix} = \begin{bmatrix} \mathbf{H}_\theta & \mathbf{O} \\ \mathbf{O} & \mathbf{H}_\sigma \end{bmatrix} \begin{bmatrix} \boldsymbol{\nu}_\theta \\ \boldsymbol{\nu}_\sigma \end{bmatrix}. \tag{10}$$

Table 1
The dimensions of the current prototype of the McGill SMG.

Dimensions	l_0	l_1	l_2	l_3	a_{II4}	a_{II5}	a_1	t
Values (m)	0.6	0.06	0.6329	0.3	0.0621	0.0254	0.12	0.03

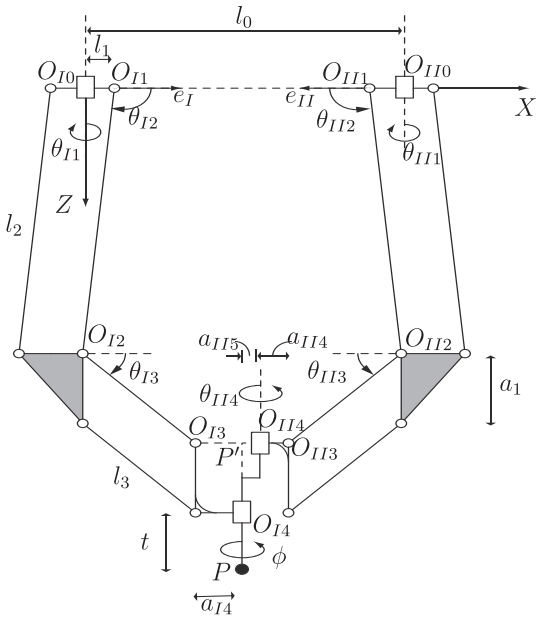

Fig. 2. Front view of the kinematic chain of the McGill SMG at the reference pose.

Thus, by substitution of Eqs. (9) and (10) into Eqs. (4b) and (4a), respectively, the force and moment vectors are transformed into dimensionless parameter vectors by means of new linear transformations,

$$\mathbf{f} = \mathbf{G}_f \psi, \quad \mathbf{n} = \mathbf{G}_n \boldsymbol{\nu} \tag{11}$$

in which $\mathbf{G}_f$ and $\mathbf{G}_n$ are dimensionally homogeneous coefficient matrices that have units corresponding to $\mathbf{f}$ and $\mathbf{n}$, respectively, i.e.,

$$\begin{aligned} \mathbf{G}_f &= \begin{bmatrix} \mathbf{K}_{12}^T \mathbf{S}_\theta & \mathbf{K}_{22} \mathbf{S}_\sigma \end{bmatrix}, \quad \psi = \begin{bmatrix} \psi_\theta^T & \psi_\sigma^T \end{bmatrix}^T \\ \mathbf{G}_n &= [\, \mathbf{K}_{11} \mathbf{H}_\theta \quad \mathbf{K}_{12} \mathbf{H}_\sigma \,], \quad \boldsymbol{\nu} = \begin{bmatrix} \boldsymbol{\nu}_\theta^T & \boldsymbol{\nu}_\sigma^T \end{bmatrix}^T. \end{aligned} \tag{12}$$

Both matrices $\mathbf{G}_f^T \mathbf{G}_f$ and $\mathbf{G}_n^T \mathbf{G}_n$ have three mutually orthogonal eigenvectors corresponding to three non-zero eigenvalues that characterize the distortion of the unit spheres $\|\mathbf{f}\| = 1$ (N) and $\|\mathbf{n}\| = 1$ (Nm), respectively. The minimum values of the eigenvalues of

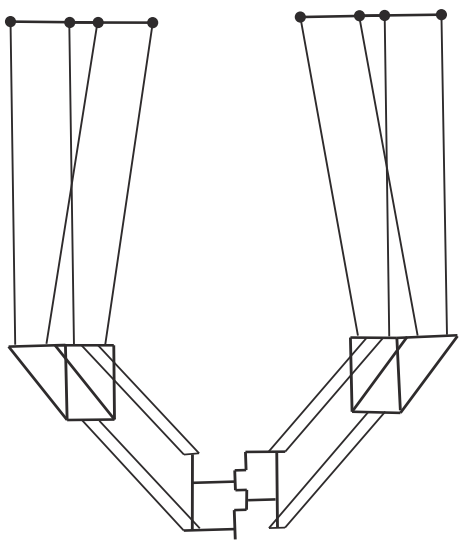

Fig. 3. The simplified model of the McGill SMG robot.

Table 2
The objectives and volume of the current McGill SMG.

κ_t^0 (N)	κ_r^0 (Nm)	Volume^{0}m^3
291.63	10.09	0.68

$\mathbf{G}_f^T\mathbf{G}_f$ and $\mathbf{G}_n^T\mathbf{G}_n$, λ_i and μ_i, $i = 1, \ldots, 3$, respectively, are now defined as translational κ_t and rotational κ_r stiffness performance indices, respectively, i.e.,

$$\kappa_t = \min_i\left(\sqrt{\lambda_i}\right), \quad \kappa_r = \min_i\left(\sqrt{\mu_i}\right), \quad i = 1, \ldots, 3 \tag{13}$$

where the square roots have been introduced because of the quadratic nature of $\mathbf{G}_f^T\mathbf{G}_f$ and $\mathbf{G}_n^T\mathbf{G}_n$.

5. The multi-objective optimization of the McGill SMG

5.1. Problem definition

This work aims to modify the link lengths of the McGill SMG in order to increase its translational and rotational stiffnesses when its MP is at a specific pose, called the *reference pose*, denoted by $\mathcal{P}$. The pose of the MP of the current prototype when it is at the home posture is considered as $\mathcal{P}$. The home posture of the robot is defined as the posture farthest from parallel singularities, as reported by Alizadeh et al. [26]. The joint angles of the current McGill SMG at the home posture are:

$$\theta_{I1} = \theta_{II1} = 0, \quad \theta_{I2} = \theta_{II2} = 5.28^\circ, \quad \theta_{I3} = \theta_{II3} = 45^\circ, \quad \theta_{I4} = 0, \quad \theta_{II4} = 180^\circ. \tag{14}$$

Hence, with the current dimensions, shown in Table 1, the reference pose $\mathcal{P}$ is obtained as

$$\mathcal{P} : (X_\mathcal{P}, Y_\mathcal{P}, Z_\mathcal{P}, \phi_\mathcal{P}) = \left(\frac{l_0}{2}, 0, 0.991, 0\right). \tag{15}$$

At this reference pose, the robot is symmetric with respect to a plane parallel to the *ZY*-plane passing from the reference pose $\mathcal{P}$. In this problem, six dimensions all affect significantly the stiffness of the robot; l_0: the distance between two limbs, l_2: the length of the proximal $\prod$-joints, l_3: the length of the distal $\prod$-joints, a_{I4}, a_{II4}, and a_{I5}: the dimensions at the moving platform level where it is connected to the distal $\prod$-joints by means of the wrist brackets. These six dimensions are shown in Fig. 2. At the reference pose, it is assumed that the robot is maintained symmetric with respect to the *ZY*-plane; hence, the joint angles that define $\mathcal{P}$ are

$$\theta_{I1} = \theta_{II1} = 0, \quad \theta_{I2} = \theta_{II2} \quad \theta_{I3} = \theta_{II3}, \quad \theta_{I4} = 0, \quad \theta_{II4} = 180^\circ \tag{16}$$

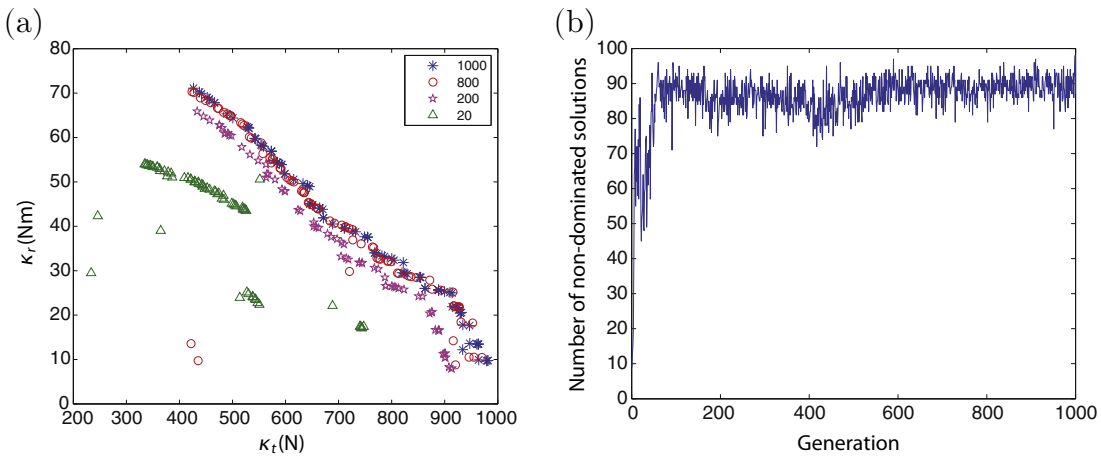

Fig. 4. (a) The convergence of the Pareto frontier after 20, 200, 800 and 1000 generations; and (b) The number of non-dominated solutions with respect to the generation number.

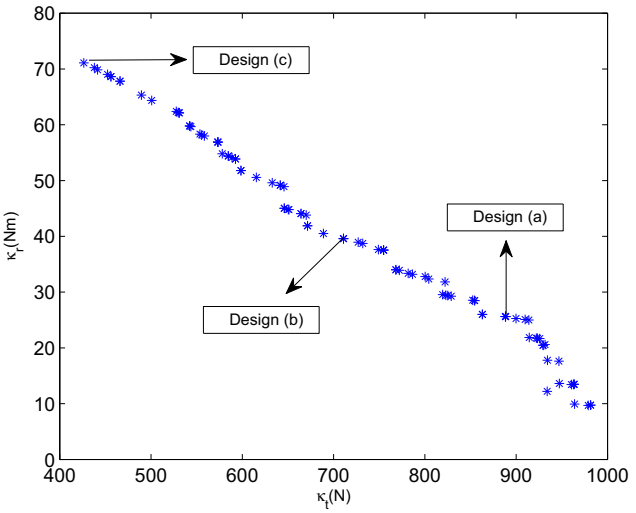

Fig. 5. The Pareto frontier obtained after 1000 generations.

whence,

$$a_{I4} = a_{II4} + a_{II5}. \tag{17}$$

Therefore, only five dimensions are independent, which are the design variables. The translational and rotational stiffness indices, κ_t and κ_r, defined in Section. 4.1 are chosen as the objective functions to be maximized when the McGill SMG is at its home posture. Accordingly, the design variable vector **x** and the objective vector **f** are:

$$\mathbf{x} = [\, l_0 \quad l_2 \quad l_3 \quad a_{II4} \quad a_{II5} \,]^T, \quad \mathbf{f} = [\, \kappa_t \quad \kappa_r \,]^T. \tag{18}$$

By resorting to the constraints in Eq. (16), at the proposed reference position, lengths l_2 and l_3 can be obtained in terms of θ_{I2} and θ_{I3}, namely,

$$l_2 = \frac{(a_1 + t - B_z)cos\theta_{I3} - (l_1 + a_{I4} - l_0/2)sin\theta_{I3}}{sin(\theta_3 - \theta_2)} \tag{19}$$

$$l_3 = \frac{(a_1 + t - B_z)cos\theta_{I2} - (l_1 + a_{I4} - l_0/2)sin\theta_{I2}}{sin(\theta_2 - \theta_3)}. \tag{20}$$

Parameters a_1, t and l_1 are constant, and equals to the values used in the current prototype (Table 1). For each set of design variables, in order to calculate the objectives, θ_{I2} and θ_{I3} should be obtained by solving the trigonometric Eqs. (19) and (20). In this

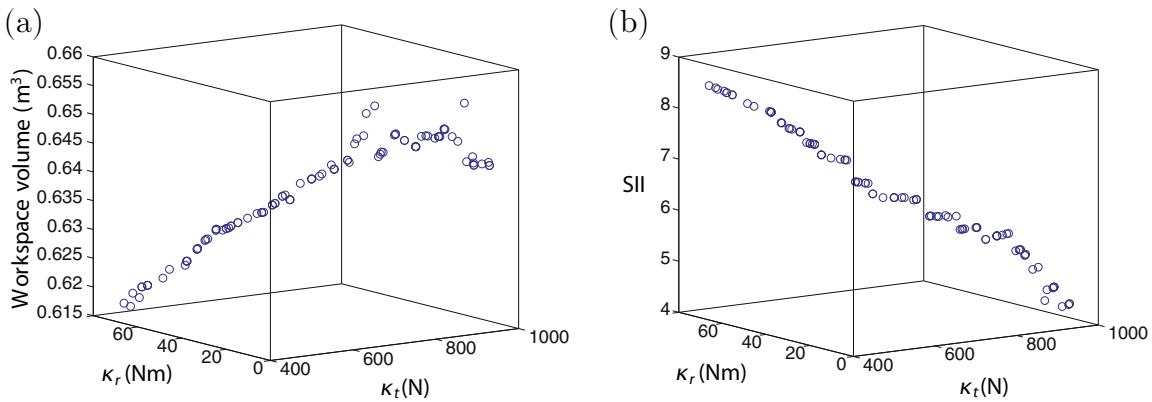

Fig. 6. (a) The workspace volume and (b) the SII of the Pareto frontier members.

Table 3
The specifications of the three different designs of the McGill SMG.

Specifications	Design (a)	Design (b)	Design (c)
l_0 (m)	0.6988	0.6988	0.6988
l_2 (m)	0.4533	0.4875	0.5804
l_3 (m)	0.4487	0.4092	0.3017
a_{II4} (m)	0.0241	0.0254	0.0497
a_{II5} (m)	0.0471	0.0673	0.0986
κ_t (N)	888.2773	710.8583	426.4656
κ_r (Nm)	25.6186	39.5903	71.0951
V (m^3)	0.6452	0.6398	0.6178
SII	5.5854	6.3621	8.5099

optimization procedure, as a beneficial alternative, instead of l_2 and l_3, θ_{I2} and θ_{I3} can be directly used as design variables. In other words, the variables l_2 and l_3 are changed via the variation of θ_{I2} and θ_{I3}. The significant merit of this alternative is that there is no need to solve the trigonometric equations at each step, which makes the optimization procedure faster and more accurate. Hence, the design-variable vector becomes

$$\mathbf{x} = [\, l_0 \quad \theta_{I2} \quad \theta_{I3} \quad a_{II4} \quad a_{II5} \,]^T. \tag{21}$$

The design-variable lower and upper bounds are defined as:

$$0.5\text{m} \le l_0 \le 0.7\text{m}$$
$$90^\circ \le \theta_{I2} \le 130^\circ$$
$$30^\circ \le \theta_{I3} \le 60^\circ$$
$$0.02\text{m} \le a_{II4} \le 0.05\text{m}$$
$$0.01\text{m} \le a_{II5} \le 0.1\text{m}.$$

6. Numerical results

When adopting the NSGA-II procedure, the maximum number of generation is set as 1000, each made of 100 individuals. The terms generation and individual in the GAs stand for loop and design. Hence, in the foregoing optimization procedure, the maximum number of 1000 loops is run, in each loop containing 100 different designs. The crossover, where two parents mate to produce children, is performed via the simulated binary crossover (SBX) operator [27]. To evaluate the objectives, the simplified model of the McGill SMG is used.

In this model, depicted in Fig. 3, the proximal ∏ joints are modeled by aluminum frames instead of complex composite boxes. As GA multi-objective optimization is a stochastic, time-demanding procedure, the objective evaluations inside the algorithm can tremendously slow it down. Using a simplified model makes the evaluation process much faster so as to be able to conduct a less time-consuming, yet complete search procedure. This also helps to see solely the effect of the dimensions on the robot stiffness. For the simplified model of the McGill SMG with the current dimensions, the values of κ_t and κ_r and the workspace volume are shown in Table 2. The optimization procedure is run for a maximum of 1000 generations with the crossover and mutation probabilities of 80% and 5%, respectively. This means that, at each generation, 80% of the individuals mate, while the remained 20% are transferred directly to the next generation; and 5% of the children undergo random mutations in order to conduct a complete search on the design-variable space. As the number of generations is increased, the final individuals approach the Pareto optimal set and the corresponding objective to the Pareto frontier. In Fig. 4(a), the evolution of the objectives trade-off after 20, 200, 800 and 1000 generations is plotted. Apparently, the

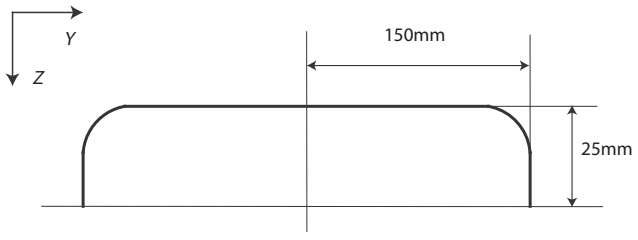

Fig. 7. The smoothed test trajectory proposed by [28].

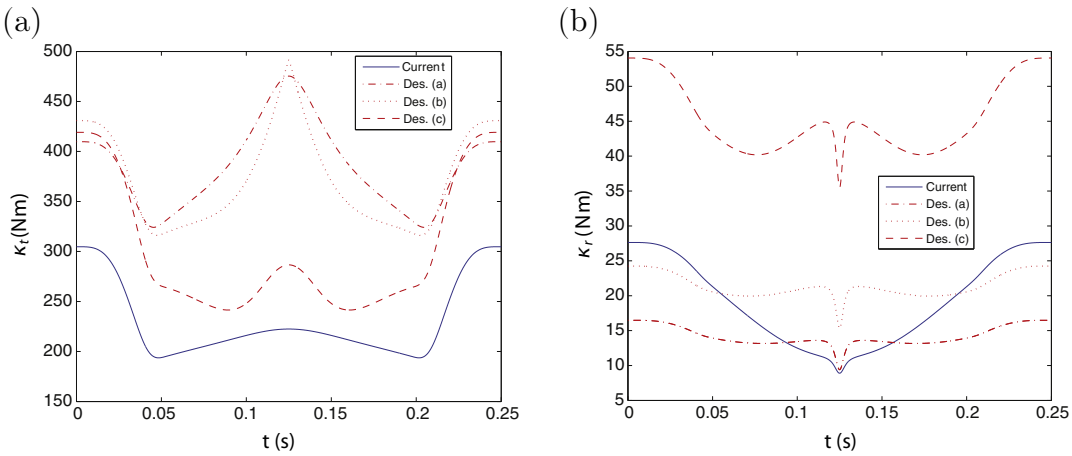

Fig. 8. The evolution of (a) translational κ_t and (b) rotational κ_r stiffness indices for three different.

objective trade-off variation from the generation number 800 to 1000 is almost trivial. Moreover, Fig. 4(b) shows the number of non-dominant solutions with respect to the number of generations. The percentage of non-dominant solutions to the total number of individuals at each generation can be regarded as the closeness of the individuals to the actual Pareto optimal set. Apparently, after 600 generations, at each generation, in the average, 90% of individuals are non-dominant; this implies a satisfactory convergence of the individuals to the actual Pareto optimal set. For the maximum number of 1000 generations, the Pareto frontier obtained is shown in Fig. 5. The Pareto optimal set contains number of designs none of which dominates others; hence, in order to select one of them as a final design, other criterion is needed. An appropriate combination of objective functions can be considered as a criterion. For example, here, a new index κ which is called the *stiffness improvement index* (SII) is defined:

$$\kappa = \frac{\kappa_t}{\kappa_t^0} + \frac{\kappa_r}{\kappa_r^0} \tag{22}$$

in which κ_t^0 and κ_r^0 are the translational and rotational stiffness indices of a reference design. In our optimization problem, the simplified model of the McGill SMG, depicted in Fig. 3, with the current dimensions is considered as a reference design, and κ_t^0 and κ_r^0 are calculated

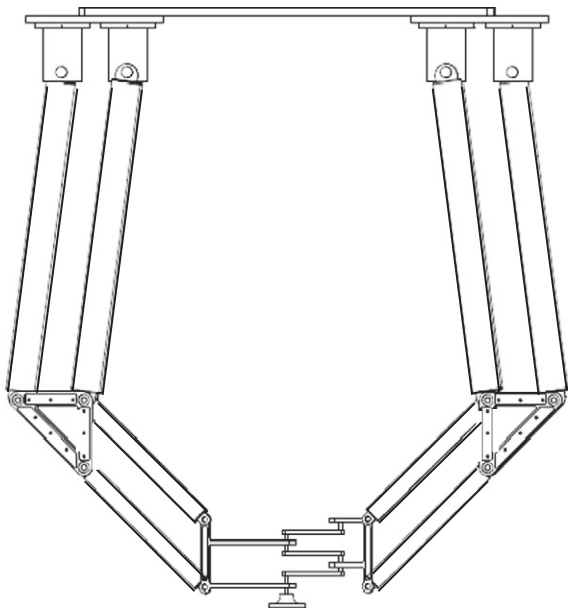

Fig. 9. The McGill SMG with optimum dimensions.

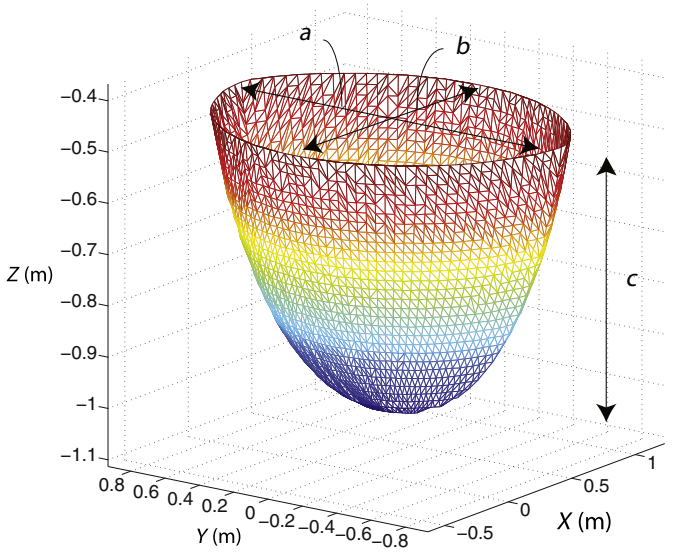

Fig. 10. The workspace of the McGill SMG with optimum dimensions, $a = 1.84$ m, $b = 1.48$ m and $c = 0.64$ m.

at its home posture. In addition to SII, the workspace volume also can be used as a criterion. Both criteria, the workspace volume and the SII, of the Pareto frontier members are monitored in Fig. 6(a) and (b). The workspace volume has a minimum and maximum of 0.61 m^3 and a 0.66 m^3, respectively. Compared to the workspace volume of the current prototype, which is 0.68 m^3, all the members of the

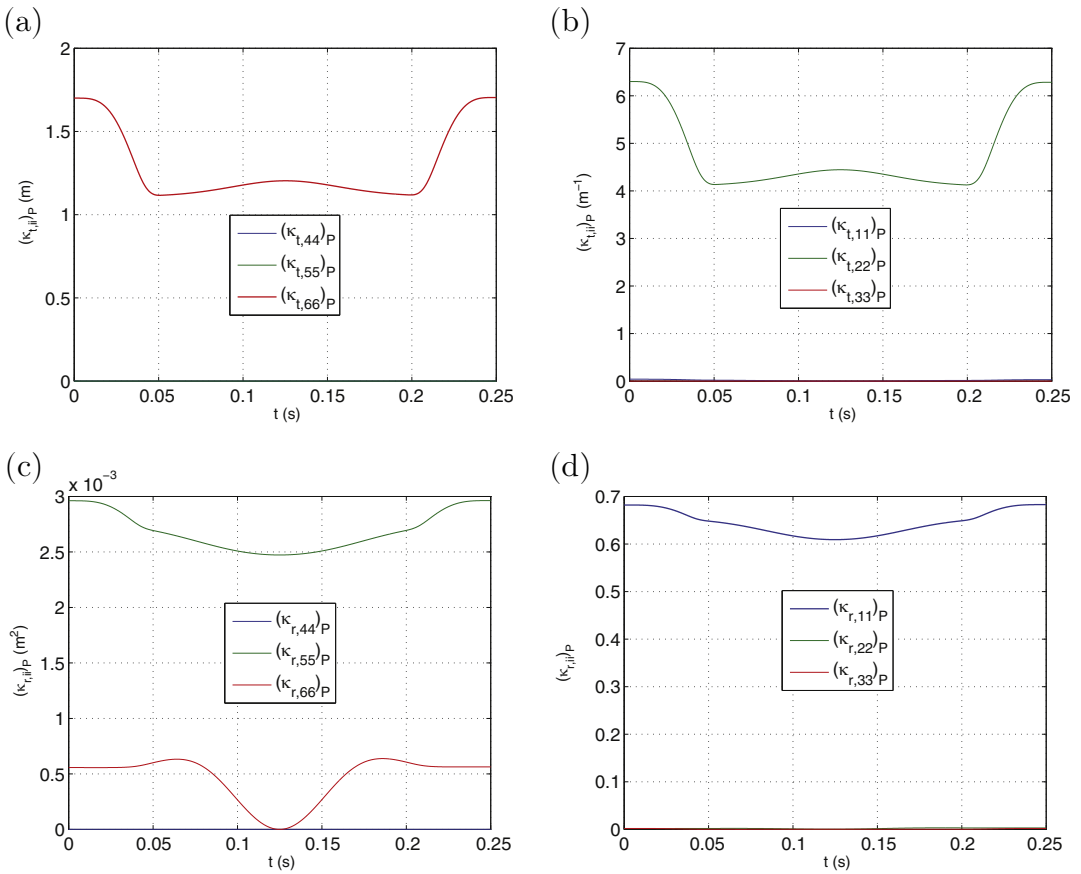

Fig. 11. The sensitivity of κ_t and κ_r to the diagonal entries of the proximal ∏-joint over the smoothed test trajectory: (a) $(\kappa_{t,ii})_P$; (b) $(\kappa_{t,ii})_P$; (c) $(\kappa_{r,ii})_P$; (d) $(\kappa_{r,ii})_P$.

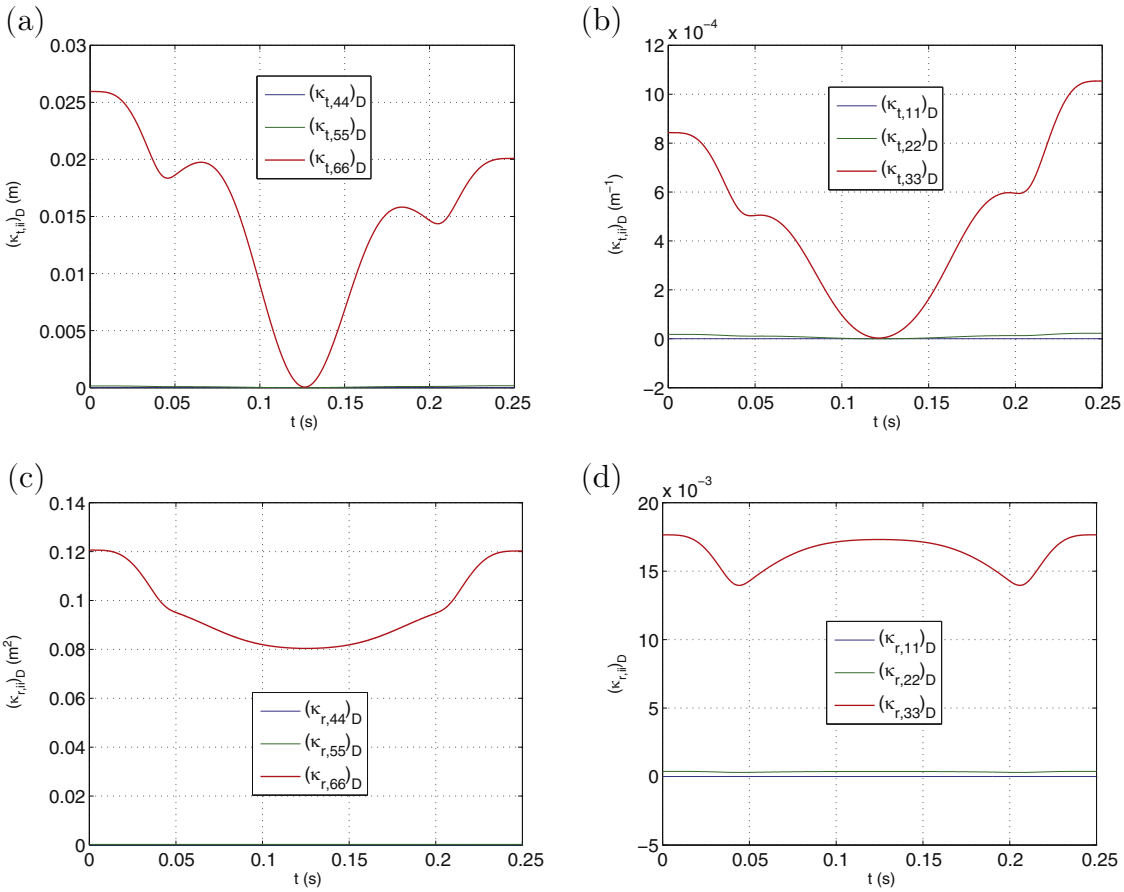

Fig. 12. The sensitivity of κ_t and κ_r to the diagonal entries of the distal ∏-joint over the smoothed test trajectory: (a) $(\kappa_{t,ii})_D$; (b) $(\kappa_{t,ii})_D$; (c) $(\kappa_{r,ii})_D$; (d) $(\kappa_{r,ii})_D$.

Pareto frontier, in terms of the size of workspace, are acceptable. However, the SII changes in a broad range from a minimum value of 4 to the maximum of 9. Although the SII value provides a good measurement of the overall stiffness improvement, a design with a large SII is not necessarily the best. To ensure that it is, in addition to the design with a maximum SII, design (c), two members of the Pareto optimal set, designs (a) and (b), with different values of SII are arbitrarily chosen; the features of these designs are shown in Table 3.

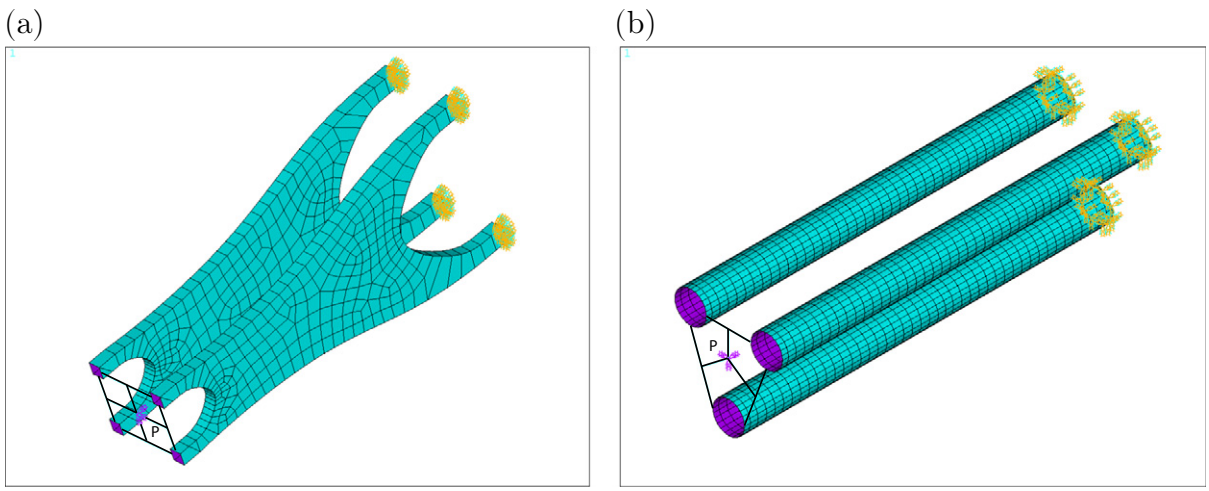

Fig. 13. Two design variants of the proximal ∏-joint: (a) Two composite boxes; (b) Three composite tubes.

Table 4
Properties of LTM25 unidirectional prepreg [29].

Fiber direction modulus (E_x)	126.2 GPa
Matrix direction modulus (E_y)	10 GPa
Shear modulus (E_s)	2.14 GPa
Poisson ratio (ν_x)	0.3
Density (ρ)	1547 kg/m^3
Ply thickness (h_0)	0.17 mm

Now, to compare the designs (a), (b) and (c), the stiffness performance indices while going through a pick-and-place operation following a standard test trajectory are calculated. This trajectory involves a 25 mm vertical upward translation, a 300 mm horizontal translation, and a 25 mm downward vertical translation. Moreover, the MP should follow this trajectory with a rotation of 180° while moving along the horizontal segment. Here, we use the smoothed test trajectory proposed by Gauthier et al. [28], as displayed in Fig. 7. The evolutions of the two objective functions κ_t and κ_r for the design with current dimensions and three optimum designs are plotted in Fig. 8(a) and (b). Apparently, design (c) shows a significant improvement of κ_r over the test trajectory while designs (a) and (b) are even weaker than the design with the current dimensions. Although designs (a) and (b) show a greater translational stiffness with respect to the others, because of the weak rotational stiffnesses in some part of the trajectory, they are failed to be chosen. Hence, the dimensions of design (c), which is the best, in terms of the rotational stiffness index, and better than the design with the current dimensions in terms of the translational stiffness index, is selected as the optimum solution. The 2D sketch of the McGill SMG with optimum dimensions is depicted in Fig. 9. The workspace of the robot with the optimum dimensions is plotted in Fig. 10. With the workspace volume of 0.62 m^3, the McGill SMG with optimum dimensions still has a larger workspace than its competitor the Adept's Quattro with its workspace volume of 0.52 m^3.

7. Stiffness sensitivity analysis of the McGill SMG

The 6 × 6 stiffness matrix of a flexible part, proximal or distal ∏-joints, $\mathbf{K}_P$ or $\mathbf{K}_D$, respectively, contains 36 components of which only 21 are independent, because of the inherent symmetry of the stiffness matrices. However, the effect of components on the robot stiffness in a direction is not similar. This calls for a stiffness sensitivity analysis on the McGill SMG. In this analysis, first, the objectives related to the stiffness of a system are defined; then, the sensitivity of these objective functions to the variation of the system variables is obtained. This study aims to obtain the sensitivity of the two stiffness indices, translational κ_t and rotational κ_r, to the six diagonal components of the Cartesian stiffness matrix of the proximal and distal ∏-joints, namely,

$$\left(\kappa_{j,ii}\right)_P = \frac{\partial \kappa_j}{\partial k_{P,ii}}, \quad \left(\kappa_{j,ii}\right)_D = \frac{\partial \kappa_j}{\partial k_{D,ii}}, \quad j = t, r \quad i = 1\ldots3, \tag{23}$$

where $k_{P,ii}$ and $k_{D,ii}$ $i = 1 \ldots 6$ are the diagonal components of the proximal and distal ∏-joints stiffness matrices, respectively. Although all 21 components of each flexible part stiffness matrix affect the stiffness indices, the effect of six diagonal components is more significant. Here, by resorting to the finite difference method, the stiffness sensitivity analysis of the McGill SMG with the optimum dimensions, obtained in the previous section, is conducted. As the number of objectives is two and the number of design variables are 12, the analysis results in 24 sensitivity values.

Now, while the McGill SMG is operating through the smoothed test trajectory, $(\kappa_{j,ii})_P$ and $(\kappa_{j,ii})_D$ where $j = t,r$ and $i = 1 \ldots 3$, are calculated. The units of κ_t and κ_r are N and Nm, respectively; as the first and second three diagonal components of a stiffness matrix, corresponding to the rotational and translational motions, have units of N and N/m, respectively, the 24 sensitivity values are divided into four sets with different units. Fig. 11(a)–(d) shows the 12 sensitivity values regarding the proximal ∏-joints; apparently, $(\kappa_{t,66})_P$, $(\kappa_{t,22})_P$, $(\kappa_{r,55})_P$, and $(\kappa_{r,11})_P$ are significant. The results corresponding to the distal ∏-joint counterparts are shown in Fig. 12(a)–(d). As the results show, in the McGill SMG with the new dimensions, the four diagonal entries of the proximal ∏-joint stiffness matrix $k_{P,55}$, $k_{P,66}$, $k_{P,11}$, $k_{P,22}$ and the two of the distal ∏-joints $k_{D,66}$ and $k_{D,33}$ play critical roles. In other words, the translational stiffness of both types of ∏-joints along the *X*-axis, $k_{P,44}$ and $k_{D,44}$, do not affect the robot stiffness significantly, while the bending stiffnesses in the *ZY*-plane of

Table 5
The four effective stiffness components of the proximal ∏-joints.

Stiffness component	Two boxes	Three tubes
$k_{P,55}$ (N/m)	0.8×10^4	6.9×10^4
$k_{P,66}$ (N/m)	19.6×10^4	7.5×10^4
$k_{P,11}$ (Nm)	348.4	318.3
$k_{P,22}$ (Nm)	362.2	353.6
Mass (kg)	0.275	0.284

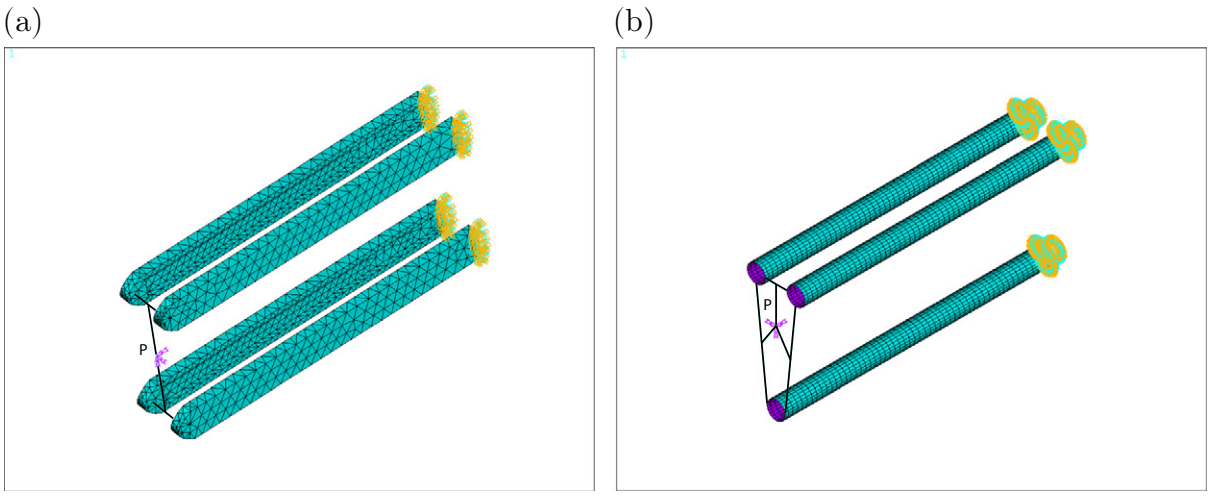

Fig. 14. Two design variants of the distal ∏-joint: (a) four aluminum bars; (b) three composite tubes.

both ∏-joints, $k_{P,66}$ and $k_{D,66}$, are important variables. Moreover, by comparing the results, apparently, the stiffness of the proximal ∏-joints affects the overall stiffness of the robot more than the distal ∏-joint. Hence, the six components, $k_{P,55}$, $k_{P,66}$, $k_{P,11}$, $k_{P,22}$, $k_{D,66}$ and $k_{D,33}$, can be considered as performance indices by which different designs of the proximal and distal ∏-joints can be compared. In the sequel, two designs for the proximal and two for the distal ∏-joints are evaluated; by comparing the proposed objectives, the best design can be recognized.

7.1. Two design variants for the proximal ∏-joints

In the current prototype, the proximal ∏-joints are made of two parallel identical trapezoid boxes made of composite materials, depicted in Fig. 13(a). Each composite box is made of a three-layer laminate with the lay-up configuration [0/90/0]. The layers are made of LTM25 unidirectional prepreg carbon/epoxy composite material, their corresponding mechanical properties being shown in Table 4. The second design, shown in Fig. 13(b), is composed of three parallel identical tubes that are made of carbon-fiber composite materials. Each tube is made of four layers of LTM25 unidirectional prepreg carbon/epoxy with the lay-up configuration [0/90/90/0]. The four effective stiffness components, $k_{P,55}$, $k_{P,66}$, $k_{P,11}$ and $k_{P,22}$, of both designs are compared in Table 5. Apparently, except for $k_{P,55}$, the two composite boxes dominate the three tubes. However, the latter shows significantly higher $k_{P,55}$. In addition to the foregoing issues, the manufacturing of a trapezoid box is more complex than that of a tube. Hence, the proximal ∏-joint made of three composite tubes is preferred over the two composite boxes.

8. Two design variants for the Distal ∏-joints

The distal ∏-joints are the other flexible components which significantly affect the stiffness of the McGill SMG. According to the sensitivity results, although the proximal ∏-joints have more influence on the overall stiffness of the robot, the stiffness improvement of the distal ∏-joints is also a crucial matter. In the current prototype, each distal ∏-joint is made of four parallel aluminum bars, shown in Fig. 14(a), each bar is 0.3 m long. As an alternative, the four aluminum bars can be replaced with three tubes made of composite materials. In this case, each tube is made of four LTM25 unidirectional prepreg carbon/epoxy with the lay-up configuration [0/90/90/0] and a diameter of 0.03 m, as depicted in Fig. 14(b). Based on the results of a sensitivity analysis, the overall stiffness of the robot is more sensitive to the two of six diagonal entries of the distal ∏-joint stiffness matrix, $k_{D,66}$ and $k_{D,33}$. These two components of both distal ∏-joint designs are compared in Table 6. Apparently, the design composed of three tubes cannot compete with their aluminum

Table 6
The two effective stiffness components of the distal ∏-joints designs.

Stiffness component	Four aluminum bars	Three composite tubes
$k_{D,66}$ (N/m)	50.6×10^4	11×10^4
$k_{D,33}$ (N/m)	7179.6	127.8
Mass (kg)	0.3	0.09

Fig. 15. The new design of the McGill SMG robot with proximal ∏-joints made of carbon-fiber composite tubes.

counterpart; however, the former is much lighter than the latter. Even if the number of layers is increased to eight, the stiffness components are still much lower than that of the aluminum bars. Therefore, the distal ∏-joint with four aluminum bars is recommended to remain in the new design.

9. The CAD model of the new designs

Figs. 15 and 16 are the CAD model of the two recommended designs of the McGill SMG with optimum dimensions. In the former design, the proximal ∏-joints are made of carbon-fiber composite tubes and the distal ∏-joints are made of aluminum bars, while in the latter, both type of the ∏-joints are composed of carbon-fiber tubes.

Fig. 16. The new design of the McGill SMG robot with proximal and distal ∏-joints made of carbon-fiber composite tubes.

The design depicted in Fig. 15 is expected to be stiffer than its counterpart shown in Fig. 16, while the latter is lighter than the former. Since, in the design of the McGill SMG, the robot mass also plays an important role, there should be a compromise between the robot mass and stiffness. This provides a great opportunity as a future research to calculate the optimum design of the robot in terms of the stiffness and mass.

10. Conclusions

The stiffness optimization and sensitivity analysis of the McGill SMG was the subject of this study. By resorting to the translational and rotational stiffness indices, a multi-objective optimization problem was defined. To avoid solutions with unreasonable workspace volumes a specific condition was applied. By the use of GAs, the foregoing multi-objective optimization led to a set of Pareto optimal solutions. Each member of the Pareto optimal set can fit an additional criterion, and thus, can be considered as an optimum solution. The stiffness improvement index (SII) was defined in order to pick up a unique solution. Finally, the stiffness performance of the design with maximum SII and two other members of the Pareto optimal set over a standard test trajectory were examined, thereby finding the optimum design. At the end, a novel approach for the sensitivity analysis of flexible parallel robots, motivated by McGill SMG, was introduced.

Appendix A. Calculation of the McGill SMG stiffness matrix

The results obtained in [9] are used to calculate the stiffness matrix of the McGill SMG; the robot consists of one base platform (BP) and one moving platform (MP), the two are coupled by two limbs, shown in Fig. 1, which is modeled as the elastostatic system depicted in Fig. A.17. In this simplified model, each limb consists of two rigid links: the elbow brackets (EB), and the wrist bracket (WB). Considering the parallelograms as $\prod$-joints, the kinematic chain of the McGill SMG is thus of the R$\prod\prod$RR$\prod\prod$R type. In the elastostatic model each $\prod$-joint is replaced with its corresponding equivalent six-dimensional generalized spring. The McGill SMG has two kinds of $\prod$-joints, proximal and distal, as depicted in Fig. 1. In the actual model, each proximal $\prod$-joint includes two boxes made of composite materials, and each distal $\prod$-joint is made of four identical aluminum rods. The distal $\prod$-joints can be modeled with beam elements, while in the case of the proximal $\prod$-joints, closed-form parametric stiffness matrix is available. Because of the complex shape and the complexity associated with the modeling of composite materials, FEA was used to calculate the stiffness matrix of the composite box. However, for the optimization purposes where the robot dimensions are the design variables, the simplified model, depicted in Fig. 3, is utilized. In this model, the proximal $\prod$-joints are modeled as aluminum frames, thus, they can be modeled with beam elements as well. In the calculation of the stiffness matrix, the rigid bodies are assumed massless; hence, the potential energy only comes from elastic energy of the flexible parts, namely,

$$V = \frac{1}{2}\sum_{J=I,II}\left(\mathbf{q}_{J1}^T\left(\mathbf{K}_{22}^{PJ}+\mathbf{K}_{11}^{DJ}\right)\mathbf{q}_{J1} + 2\mathbf{q}_{J1}^T\mathbf{K}_{12}^{DJ}\mathbf{q}_{J2} + \mathbf{q}_{J2}^T\mathbf{K}_{22}^{DJ}\mathbf{q}_{J2}\right) \tag{A.1}$$

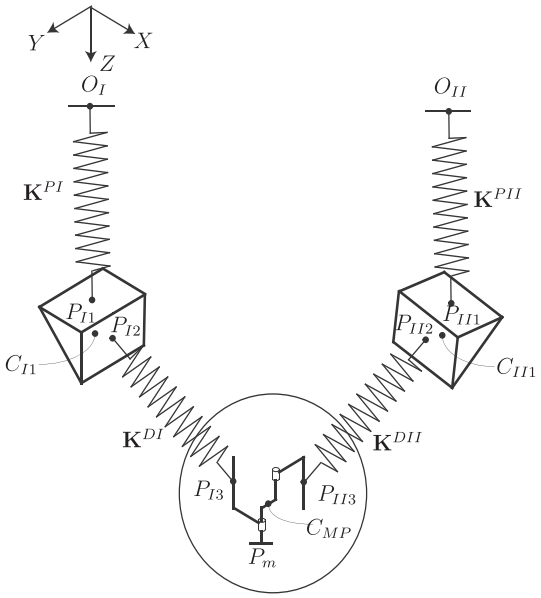

Fig. A.17. Elastostatic model of the McGill SMG.

in which $\mathbf{K}_{ij}^{PJ}$ and $\mathbf{K}_{ij}^{DJ}$ are the 6×6 block matrices of the reduced stiffness matrices of the proximal and distal $\prod$-joints, respectively, of limb J, which were derived by Taghvaeipour et al. [9]. Moreover, $\mathbf{q}_{J1}$ and $\mathbf{q}_{J2}$ are the SAD screws defined at the center of mass of the EB and WB of Jth limb.

The wrist brackets and the MP are attached by means of revolute joints, depicted in Fig. A.17 and zoomed-in in Fig. A.18; by invoking the rigidity assumption and because of the presence of the revolute joints, one has

$$\mathbf{q}_{J2} = \mathbf{G}_J\left(\mathbf{H}_J\mathbf{q}_m + \gamma_J\zeta\right), \quad \zeta = \begin{bmatrix}\mathbf{e}_\gamma^T & \mathbf{0}^T\end{bmatrix}^T \tag{A.2}$$

in which 0 is the three-dimensional zero vector, γ_J is the "small"-amplitude angle of rotation of the revolute joint of the Jth limb, and $\mathbf{e}_\gamma$ is the unit vector parallel to the revolute joint axis, which, in this case, is $[0 \quad 0 \quad 1]^T$, and hence, constant. Moreover,

$$\mathbf{G}_J = \begin{bmatrix}1 & \mathbf{O}\\ -\mathbf{A}_J & 1\end{bmatrix}, \quad \mathbf{H}_J = \begin{bmatrix}1 & \mathbf{O}\\ -\mathbf{D}_J & 1\end{bmatrix} \tag{A.3}$$

where $\mathbf{A}_J$ and $\mathbf{D}_J$ are the cross-product matrices of vectors $\mathbf{a}_J$ and $\mathbf{d}_J$, respectively [30], for $J = I, II$, as depicted in Fig. A.18. Now, Eq. (A.2) is substituted into Eq. (A.1), and hence, the potential energy of the robot becomes

$$\begin{aligned} V = \frac{1}{2}\sum_{J=I,II}\mathbf{q}_{J1}^T\left(\mathbf{K}_{22}^{PJ} + \mathbf{K}_{11}^{DJ}\right)\mathbf{q}_{J1} + 2\mathbf{q}_{J1}^T\mathbf{K}_{12}^{DJ}\mathbf{G}_J\left(\mathbf{H}_J\mathbf{q}_m + \gamma_J\zeta\right)\\ + \left(\mathbf{H}_J\mathbf{q}_m + \gamma_J\zeta\right)^T\mathbf{G}_J^T\mathbf{K}_{22}^{DJ}\mathbf{G}_J\left(\mathbf{H}_J\mathbf{q}_m + \gamma_J\zeta\right). \end{aligned} \tag{A.4}$$

After taking the gradient of the potential energy with respect to the generalized coordinates, the matrix that maps the SMG generalized displacement array into the generalized force array is obtained:

$$\begin{bmatrix}\mathbf{w}_m\\ \mathbf{w}_I\\ \mathbf{w}_{II}\\ m_{\gamma_I}\\ m_{\gamma_{II}}\end{bmatrix} = \begin{bmatrix}\mathbf{K}_{11} & \mathbf{K}_{12} & \mathbf{K}_{13} & \mathbf{K}_{14} & \mathbf{K}_{15}\\ \mathbf{K}_{12}^T & \mathbf{K}_{22} & \mathbf{O} & \mathbf{K}_{24} & 0\\ \mathbf{K}_{13}^T & \mathbf{O} & \mathbf{K}_{33} & \mathbf{0} & \mathbf{K}_{35}\\ \mathbf{K}_{14}^T & \mathbf{K}_{24}^T & \mathbf{0}^T & \mathbf{K}_{44} & 0\\ \mathbf{K}_{15}^T & \mathbf{0}^T & \mathbf{K}_{35}^T & 0 & \mathbf{K}_{55}\end{bmatrix}\begin{bmatrix}\mathbf{q}_m\\ \mathbf{q}_I\\ \mathbf{q}_{II}\\ \gamma_I\\ \gamma_{II}\end{bmatrix}. \tag{A.5}$$

The block matrices of the stiffness matrix are shown below:

$$\begin{aligned} &\mathbf{K}_{11} = \mathbf{H}_I^T\mathbf{G}_I^T\mathbf{K}_{22}^{DI}\mathbf{G}_I\mathbf{H}_I + \mathbf{H}_{II}^T\mathbf{G}_{II}^T\mathbf{K}_{22}^{DII}\mathbf{G}_{II}\mathbf{H}_{II}, \quad \mathbf{K}_{12} = \mathbf{H}_I^T\mathbf{G}_I^T\mathbf{K}_{12}^{DI}\\ &\mathbf{K}_{13} = \mathbf{H}_{II}^T\mathbf{G}_{II}^T\mathbf{K}_{12}^{DII}, \quad \mathbf{K}_{22} = \mathbf{K}_{22}^{PI} + \mathbf{K}_{11}^{DI}, \quad \mathbf{K}_{24} = \mathbf{K}_{12}^{DI}\mathbf{G}_I\zeta\\ &\mathbf{K}_{33} = \mathbf{K}_{22}^{PII} + \mathbf{K}_{11}^{DII}, \quad \mathbf{K}_{35} = \mathbf{K}_{12}^{DII}\mathbf{G}_{II}\zeta\\ &\mathbf{K}_{44} = \zeta^T\mathbf{G}_I^T\mathbf{K}_{22}^{DI}\mathbf{G}_I\zeta, \quad \mathbf{K}_{55} = \zeta^T\mathbf{G}_{II}^T\mathbf{K}_{22}^{DII}\mathbf{G}_{II}\zeta. \end{aligned} \tag{A.6}$$

The Cartesian stiffness matrix is a mapping between the SAD of the MP and the actuator wrench applied onto it, namely,

$$\mathbf{w}_I = \mathbf{w}_{II} = 0. \tag{A.7}$$

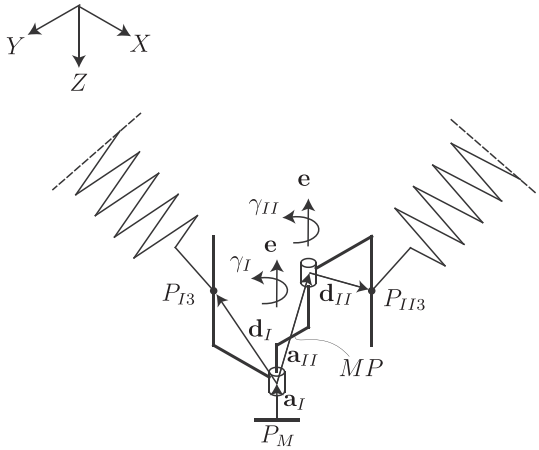

Fig. A.18. A zoom-in of the MP and the wrist brackets in the elastostatic model of the McGill SMG.

Moreover, the passive revolute joints transmit a zero moment about their axes. Hence, the 6×6 Cartesian stiffness matrix of the overall robot becomes, finally,

$$\mathbf{K}_e = \mathbf{K}_{11} - \begin{bmatrix} \mathbf{K}_{12}^T & \mathbf{K}_{13}^T & \mathbf{K}_{14}^T & \mathbf{K}_{15}^T \end{bmatrix} \begin{bmatrix} \mathbf{K}_{22} & \mathbf{O} & \mathbf{K}_{24} & 0 \\ \mathbf{O} & \mathbf{K}_{33} & \mathbf{0} & \mathbf{K}_{35} \\ \mathbf{K}_{42} & \mathbf{0}^T & \mathbf{K}_{44} & 0 \\ \mathbf{0}^T & \mathbf{K}_{53} & 0 & \mathbf{K}_{55} \end{bmatrix}^{-1} \begin{bmatrix} \mathbf{K}_{12} \\ \mathbf{K}_{13} \\ \mathbf{K}_{14} \\ \mathbf{K}_{15} \end{bmatrix} \tag{A.8}$$

which relates the SAD of the MP, defined at point P_M, to the wrench applied onto the MP, with the force acting along a line that passes through P_M.

References

[1] D. Goldberg, Genetic Algorithms in Search and Machine Learning, Addison Wessley, Reading, MA, 1989.
[2] C. Kirkpatrick, S. Gellat, M. Vecchi, Optimization by simulated annealing, Science 220 (1983) 671–680.
[3] M. Box, A new method of constraint optimization and a comparison with other methods, Comput. J. 8 (1965) 42–52.
[4] K. Stock, M. Miller, Optimal kinematic design of spatial parallel manipulators: application to linear delta robot, ASME J. Mech. Des. 125 (2003) 292–301.
[5] C. Ceccarelli, M. Lanni, A multi-objective optimum design of general 3r manipulators for prescribed workspace limits, Mech. Mach. Theory 39 (2004) 119–132.
[6] Z.-L. Liu, X.-J. Jen, F. Gao, Optimum design of 3-DOF spherical parallel manipulators with respect to the conditioning and sti€ness indices, Mech. Mach. Theory 35 (2000) 1257–1267.
[7] D. Gao, Z. Zhang, Y. Ge, Design optimization of a spatial six degree-of-freedom parallel manipulator based on artificial intelligence approaches, Robot. Comput. Integr. Manuf. 26 (2010) 180–189.
[8] O. Kelaiaia, R. Company, A. Zaatri, Multiobjective optimization of a linear delta parallel robot, Mech. Mach. Theory 50 (2012) 159–178.
[9] A. Taghvaeipour, J. Angeles, L. Lessard, On the elastostatic analysis of multibody systems, Mech. Mach. Theory 58 (2012) 202–216.
[10] K. Deb, Multi-Objective Optimization Using Evolutionary Algorithms, John Wiley and Sons, Chichester, England, 2001.
[11] I. Rechenberg, Evolutionsstrategie: Optimierung technischer Systeme nach Prinzipien der biologischen Evolution, Frommann-Holzboog, Stuttgart, 1973.
[12] H. Holand, Adaptation in natural and artificial systems: an introductory analysis with applications to biology, control, and artificial intelligence, U Michigan Press, Oxford, England, 1975.
[13] J. Schaffer, Multiple objective optimization with vector evaluated genetic algorithms, Proc. of the First International Conference on Genetic AlgorithmsLawrence Erlbaum Associates Inc., Hillsdale, NJ, 1985, pp. 93–100.
[14] M. Fourman, Compaction of symbolic layout using genetic algorithms, Proc. of the First International Conference on Genetic AlgorithmsLawrence Erlbaum Associates Inc., Hillsdale, NJ, 1985, pp. 141–153.
[15] E. Zitzler, Evolutionary Algorithms for Multiobjective Optimization: Methods and Applications, Ph.D. thesis Swiss Federal Institute of Technology, ETH, Zurich, 1999.
[16] K. Srinivas, N. Deb, Multiobjective optimization using nondominated sorting in genetic algorithms, Evol. Comput. 2 (3) (1994) 221–248.
[17] S.M.-T. Deb, K. Agrawal, A fast elitisit multiobjective genetic algorithm: NSGA-II, IEEE Trans. Evol. Comput. 6 (2) (2002) 182–197.
[18] C. Corradini, J.C. Fauroux, S. Krut, O. Company, Evaluation of a 4-degree of freedom parallel manipulator stiffness, Proc. of the 11th World Congress in Mechanism and Machine Science, August 18–21, China2003.
[19] C. Gosselin, Stiffness mapping for parallel manipulator, IEEE Trans. Robot. Autom. 6 (1990) 377–382.
[20] A. Pashkevich, D. Chablat, Stiffness analysis of multi-chain parallel robotic systems, 9th IFAC Workshop on Intelligent Manufacturing Systems, October 9–10, Szczecin, Poland, 2008.
[21] D. Deblaise, X. Hernot, P. Maurine, A systematic analytical method for PKM stiffness matrix calculation, Proc. 2006 IEEE International Conference on Robotics and Automation, May 15–19, Orlando, USA2006.
[22] J. Lončarić, The normal forms of a stiffness matrix and compliance matrices, IEEE J. Robot. Autom. RA-3 (6) (1987) 567–572.
[23] J. Hervé, F. Sparacino, Star, a new concept in robotics, Proc. 3rd Int. Workshop on Advances in Robot Kinematics, September 7–9, Ferara, Italy, 1992.
[24] K. Wohlhart, Displacement analysis of the general spatial parallelogram manipulator, Proc. 3rd Int. Workshop on Advances in Robot Kinematics, September 7–9, Ferara, Italy, 1992, pp. 104–111.
[25] J. Kovecses, S. Ebrahimi, Parameter analysis and normalization for the dynamics and design of multibody systems, J. Comput. Nonlinear Dyn. 4 (2009) 031008-1–031008-10.
[26] D. Alizadeh, J. Angeles, S. Nokleby, On the computataion of the home posture of the McGill Schönflies-motion generator, Proc. 5th Int. Workshop on Computational Kinematics, May 6–8, Duisburg, Germany2009.
[27] R. Deb, K. Agrawal, Simulated binary crossover for continuous search space, Complex Syst. 9 (1995) 115–148.
[28] J.-F. Gauthier, J. Angeles, S. Nokleby, Optimization of a test trajectory for SCARA systems, Adv. Robot Kinematics Anal. Des. 4 (2008) 225–234.
[29] I.M. Daniel, O. Ishai, Engineering Mechanics of Composite Materials, Oxford University Press, New York, 1994.
[30] J. Angeles, Fundamentals of Robotic Mechanical Systems Theory, Methods, and Algorithms, Springer, NY, USA, 2007..